Inorganic Chemistry

Article

pubs.acs.org/IC

Comparative Insight into Electronic Properties and Reactivities toward C−H Bond Activation by Iron(IV)−Nitrido, Iron(IV)−Oxo, and Iron(IV)−Sulfido Complexes: A Theoretical Investigation

Hao Tang, Jia Guan, Huiling Liu,* and Xuri Huang*

Institute of Theoretical Chemistry, State Key Laboratory of Theoretical and Computational Chemistry, Jilin University, Changchun 130023, People's Republic of China

Supporting Information

ABSTRACT: A range of novel octahedral iron(IV)−nitrido complexes with the TMC ligand (TMC = 1,4,8,11-tetramethyl-1,4,8,11-tetraazacyclotetradecane) in the equatorial plane and one axial ligand trans to the nitrido have been designed theoretically, and a systematic comparative study of their geometries, electronic properties, and reactivities in hydrogen atom abstraction reactions regarding the iron(IV)−oxo and −sulfido counterparts has been performed using density-functional theory methods. Further, the relative importance of the axial ligands on the reactivity of the iron(IV)−nitrido systems is probed by sampling the reactions of CH_4 with $[Fe^{IV}{=}N(TMC)(L_{ax})]^{n+}$, ($L_{ax}$ = none, CH_3CN, $CF_3CO_2^-$, N_3^-, Cl^-, NC^-, and SR^-). As we find, one hydrogen atom is abstracted from the methane by the iron(IV)−nitrido species, leading to an $Fe^{III}(N)-H$ moiety together with a carbon radical, similar to the cases by the iron(IV)−oxo and −sulfido compounds. DFT calculations show that, unlike the well-known iron(IV)−oxo species with the $S = 1$ ground state where two-state reactivity (TSR) was postulated to involve, the iron(IV)−nitrido and −sulfido complexes stabilize in a high-spin ($S = 2$) quintet ground state, and they appear to proceed on the single-state reactivity *via* a dominantly and energetically favorable low-lying quintet spin surface in the H-abstraction reaction that enjoys the exchange-enhanced reactivity. It is further demonstrated that the iron(IV)−nitrido complexes are capable of hydroxylating C−H bond of methane, and potential reactivities as good as the iron(IV)−oxo and −sulfido species have been observed. Additionally, analysis of the axial ligand effect reveals that the reactivity of iron(IV)−nitrido oxidants in the quintet state toward C−H bond activation enhances as the electron-donating ability of the axial ligand weakens.

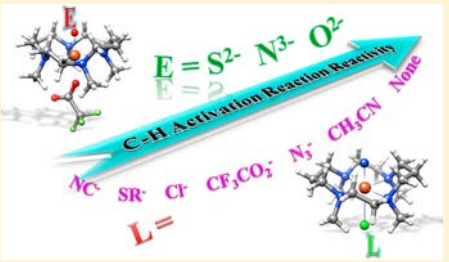

1. INTRODUCTION

Selective functionalization of unactivated C−H bonds is an extremely important industrial process in organic synthesis,[1−3] and one of the most intriguing examples is the oxidation of methane.[4] A series of metalloenzymes have been reported to fulfill such challenging targets in biology through activating dioxygen and dinitrogen with employing cheap and abundant first-row transition metals, e.g., iron, copper, and manganese.[5] Among the common cofactors of enzymes involved in oxidative processes, iron is the most widespread one.[6,7]

Many high-valent iron(IV)−oxo intermediates, ranging from enzymatic heme systems[7c,8,9] to synthetic nonheme compounds,[10−12] have attracted tremendous interest in both biological processes and laboratory research due to their reactivities toward oxygenation reactions, such as the hydroxylation of unactivated C−H bonds.[10a,13,14] Note that Que,[15] Nam,[16] Solomon,[15a] Thiel,[17] Shaik,[18] Siegbahn,[19] Baerends,[20] de Visser,[21] and Neese et al.[3,22] and their respective co-workers have made great contributions to the mechanistic analysis of C−H bond activation by heme and nonheme iron(IV)−oxo complexes.

As the analogous iron−oxo complexes, the iron−nitrido complexes have also been considered as key intermediates in many significant biological transformations, due to their appealing reactivities and great potentials in modeling nitrogen fixation *via* the nitrogenase metalloenzyme.[5,23] Notably, iron(IV)−,[24] iron(V)−,[25,26] and iron(VI)−nitrido complexes[27] have been extensively characterized by spectroscopic techniques including UV−vis and X-ray absorption spectroscopy, EXAFS analysis, Mossbauer spectroscopy, MCD spectroscopy, IR and resonance Raman spectroscopy, and NMR spectroscopy, whose electronic structures have also been studied by performing DFT calculations.[24−30] For example, Wagner and Nakamoto[28] have previously reported the photochemical generation of $[Fe^{V}(N)(TPP)]$ (TPP^{2-} = tetraphenylporphinate-(2-)) and measured its resonance Raman spectrum. Efforts in Meyer's group have for the first time obtained two species of the high-valent iron−nitride complexes by photolysis of *trans*-$[(cyclam)Fe^{III}(N_3)_2]^+$ (cyclam = 1,4,8,11-tetraazacyclotetradecane) in frozen CH_3CN. One has been identified as the photoreduced five-coordinate ferrous *trans*-$[(cyclam)Fe^{II}(N_3)]^+$, formed via homolytic Fe−N_3 bond cleavage, whereas the other is photo-oxidized *trans*-$[(N_3)(cyclam)Fe^{V}(N)]^+$, formed via homolytic N−N bond cleavage and N_2 evolution.[25a] Subsequently, the synthesis and photolysis of

Received: December 17, 2012
Published: February 20, 2013

   dx.doi.org/10.1021/ic302766f | Inorg. Chem. 2013, 52, 2684−2696

[(cyclam-ac)Fe(N_3)]$^+$ (cyclam-ac$^-$ = 1,4,8,11-tetraazacyclotetradecane-1-acetate) was initially proposed to have an $S = {}^3/_2$ spin state,[25b] and its conversion to the desired [(cyclam-ac)Fe(N)]$^+$ species and dinitrogen can be enhanced at $\lambda > 420$ nm under 80 K. However, in a following in-depth spectroscopic and theoretical work, Aliaga-Alcalde et al.[25c] elucidated the electronic structure of the fascinating high-valent systems [(cyclam-ac)Fe(N_3)]$^+$ and [(cyclam-ac)Fe(N)]$^+$, and concluded that [(cyclam-ac)Fe^V(N)]$^+$ has an anomalous orbitally degenerated $S = {}^1/_2$ ground state. In 2004, Betley and Peters[24a] synthesized and characterized the first terminal iron(IV)−nitrido complex [(PhBPiPr$_3$)Fe^{IV}(N)] which is stable in solution at room temperature through N-atom transfer via strain release by anthracene elimination from 2,3:5,6-dibenzo-7-azabicyclo[2.2.1]hepta-2,5-diene. This compound was shown to exhibit ^{15}N NMR resonances near $\delta = 952$ ppm and a ν(FeN) stretching frequency of 1034 cm^{-1}. Further, a very short Fe−N bond of 1.49 Å has been calculated by density functional theory (DFT) methods.[24c] The crystallographic characterizations of iron(IV) nitrido complexes [(TIMEN^{mes})Fe(N)]$^+$ (TIMEN^{mes} = tris[2-(3-mesitylimidazol-2-ylidene)ethyl]amine) have been reported, which are supported by bulky and flexible tris(carbene)amine ligands.[29] It is very recently reported that an iron nitrido complex supported by the phenyltris(1-tert-butylimidazol-2-ylidene)borate (L^{tBu-}) ligand has been realized by Scepaniak et al.,[30a] which presents a pseudotetrahedral geometry with an $S = 0$ ground state. This [(PhB(^{t}BuIm)$_3$)Fe^{IV}(N)] species can react with phosphines, like Ph$_3$P, but no reactivity toward protons and electrons. Most interestingly, similar to the above [(PhB(^{t}BuIm)$_3$)Fe^{IV}(N)], the synthesis of the iron(IV) nitrido complex [PhB(MesIm)$_3$Fe(N)] was achieved, where PhB(MesIm)$_3^-$ is a bulky tris(carbene)borate ligand.[30b] It is found that the reaction of a suitable hydrogen-atom donor TEMPO-H (TEMPO-H = 1-hydroxy-2,2,6,6-tetramethylpiperidine) with this iron(IV) nitrido complex leads to the formation of ammonia. Although not conclusively, mechanistic investigations suggest that at least one H-atom transfer step is involved in the reaction. However, more correlative details concerning this H-atom transfer reaction involving metal nitride complexes in solution are still not available up to now.[31]

Despite the remarkable progresses in this field, there remain a number of challenges in developing the chemistry of iron nitride complexes, especially the viable ligand design, the reactivity pattern, and mechanistic investigation of iron(IV)−nitrido complexes toward hydrogen atom transfer in solution. It is worth mentioning that extensive investigations have been devoted to the mechanistic analysis of C−H bond activation by mononuclear nonheme iron(IV)−oxo models,[32,33] even by the analogous iron(IV)−sulfido complexes, yet with little precedent.[34] Toward this end, we attempt to devise a mononuclear nonheme iron(IV)−nitrido complex where the metal ion is surrounded by a distorted octahedral coordination environment of approximately C_{2v} symmetry, including a TMC ligand (TMC = 1,4,8,11-tetramethyl-1,4,8,11-tetraazacyclotetradecane) in roughly planar geometry and one ligand in the axial position to the nitride, for which can mimic a similar ligand sphere found in the mononuclear iron(IV)−oxo complex. Moreover, a detailed H-atom abstraction mechanism involving this iron(IV)−nitrido complex has been described. To obtain more information on the relative efficiencies of the iron(IV)−nitrido oxidants, we compare their corresponding geometries, electronic properties, and reactivities with the iron(IV)−oxo and −sulfido counterparts toward H-atom abstraction reactions. In addition, the axial ligands' effect on the performances of iron(IV)−nitrido oxidants in the methane C−H activations has also been elaborated.

Here, we study with DFT calculations the alkane hydroxylation by [Fe^{IV}═O(TMC)(CF$_3$CO$_2$)]$^+$, [Fe^{IV}═S(TMC)(CF$_3$CO$_2$)]$^+$, and [Fe^{IV}═N(TMC)(CF$_3$CO$_2$)] (Scheme 1a) as well as a series of iron(IV)−nitrido complexes with various axial ligands bound [Fe^{IV}═N(TMC)(L$_{ax}$)]$^{n+}$ (L$_{ax}$ = none, CH$_3$CN, CF$_3$CO$_2^-$, N$_3^-$, Cl$^-$, NC$^-$, and SR$^-$) (Scheme 1b). Methane is sampled for the alkane to serve as a naive choice where its results can be used to model trends and to make predictions on relevant data.

Scheme 1. Methane Hydroxylation Process by Nonheme Reagents in This Work: (a) [Fe^{IV}═E(TMC)(CF$_3$CO$_2$)]$^{+/0}$ (E = O^{2-}, S^{2-}, and N^{3-}) and (b) [Fe^{IV}═N(TMC)(L$_{ax}$)]$^{n+}$ with Variable Axial Ligands (L$_{ax}$)[a]

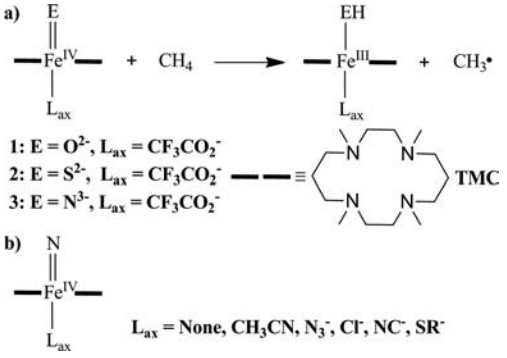

[a] L$_{ax}$ = none, CH$_3$CN, CF$_3$CO$_2^-$, N$_3^-$, Cl$^-$, NC$^-$, and SR$^-$.

2. COMPUTATIONAL METHOD

All electronic structure calculations were performed with the ORCA program package developed by the Neese group, Bonn University.[35] To take account of the solvent effect, the conductor-like screen model (COSMO) was utilized for all the calculations, and acetonitrile was chosen as the solvent. In geometric optimizations, the def2-TZVP basis sets[36] on the active atoms Fe, O, C and the transferred H atom as well as the hybrid B3LYP density functional[37] in combination with triple-ζ quality TZVP basis sets[38] on the remaining atoms were used throughout. The RIJCOSX approximation[39] was used to accelerate the calculations in combination with the auxiliary basis sets def2-TZV/J (the active atoms Fe, O, C and the transferred H atom) and TZV/J (rest).[40] This kind of basis set system is labeled as B1. These combinations of functionals/basis sets are reliable in the prediction of geometries and properties of high-valent iron complexes.[25c,27,41] All of the geometries were fully optimized without symmetry constraints. Harmonic vibrational frequencies were computed to verify the nature of the stationary points. All optimized transition states (TSs) described in this work have only one negative eigenvalue, whereas minimum structures have only positive eigenvalues of the Hessian matrix. The zero-point energies, thermal corrections, and entropy terms for the optimized geometries were obtained from the frequency calculations. The temperature and pressure for all the calculations were 298.15 K and 1.00 atm, respectively. Single point calculations were carried out with B3LYP hybrid density functional using the new default basis sets of triple-ζ quality including high angular momentum polarization functions (def2-TZVPP)[42] for all elements. The density fitting and chain of spheres (RIJCOSX) approximations have been employed together with the def2-TZVPP/J auxiliary basis set,[43] labeled as B2.

To consider dispersion forces, single-point calculations were undertaken where the semiempirical van der Waals corrections (VDW) were included.[44] Alternative functionals (B3LYP-G and

dx.doi.org/10.1021/ic302766f | Inorg. Chem. 2013, 52, 2684−2696

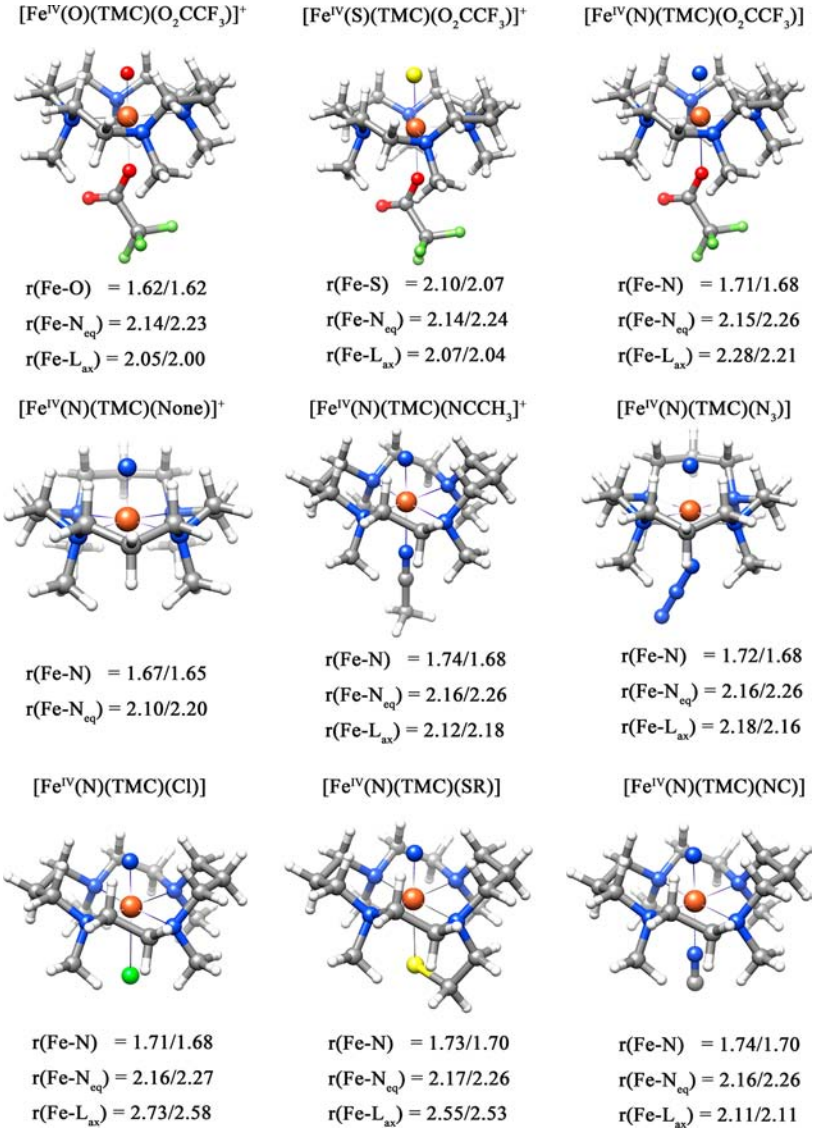

Figure 1. B3LYP/B1 optimized structures of all the complexes for the triplet and quintet states. Key bond lengths are shown for triplet/quintet states, respectively.

PBE0) were also used in single-point evaluations.[45] As expected, B3LYP-G single-point calculations gave the same trends as B3LYP and were found to not change the spin state ordering (Table S1, in the Supporting Information), since the results of the other functionals were found to be similar to B3LYP. Therefore, for simplicity, we mainly discuss the B3LYP results in the work, and collect the analogous results for the other functionals in the Supporting Information.

The bond dissociation energy of the E−H bond in the iron(IV)−hydroxo complex with ligand L_{ax} (BDE_{EH}) was calculated from eq 1 with the same methods mentioned above, namely geometry optimizations using basis set B1, while energies are taken from single-point calculations with basis set B2. Reorganization energies (RE_{FeEH}) were calculated as before from the difference in energy of the substrate in the transition state geometry and its fully relaxed structure.[18b]

$$Fe^{IV}(E)(TMC)(L_{ax}) + H \rightarrow Fe^{III}(E{-}H)(TMC)(L_{ax}) + BDE_{EH} \quad (1)$$

3. RESULTS AND DISCUSSION

We start our investigation with a detailed study of the fundamental distinctions of methane C−H activation catalyzed by iron(IV)−nitrido, −oxo, and −sulfido oxidants, respectively, where they are modeled by a TMC unit and a $CF_3CO_2^-$ axial ligand, as illustrated in Scheme 1, namely, $[Fe^{IV}{=}O(TMC)(CF_3CO_2)]^+$ (**1**), $[Fe^{IV}{=}S(TMC)(CF_3CO_2)]^+$ (**2**), and $[Fe^{IV}{=}N(TMC)(CF_3CO_2)]$ (**3**). Subsequently, the effect of axial ligands on their reactivity in methane hydroxylation is elaborated with sampling a series of axial ligands (L_{ax}) in $[Fe^{IV}{=}N(TMC)(L_{ax})]^{n+}$: L_{ax} = none, CH_3CN, $CF_3CO_2^-$, N_3^-, Cl^-, NC^-, and SR^-. Although these complexes have not yet been obtained experimentally, our selected range of axial ligands cover a much larger spread in the electron-releasing capabilities, whose properties can be comparable to those with the real iron(IV)−oxo species.[12,13a]

3.1. Comparison of $[Fe^{IV}{=}N(TMC)(CF_3CO_2)]$ to $[Fe^{IV}{=}E(TMC)(CF_3CO_2)]^+$ (E = O^{2-} and S^{2-}). Calculations on these complexes (**1**, **2**, and **3**) in both the triplet and quintet states have been performed. The geometric details in Figure 1 reveal the Fe═E bond distances of 1.62, 2.10, and 1.71 Å for cases **1**,

dx.doi.org/10.1021/ic302766f | Inorg. Chem. 2013, 52, 2684−2696

Table 1. Bond Orders and Spin Populations of the Oxidants

	Fe═E bond order[a]		Fe—N_{eq} bond order[a]		Fe—L bond order[a]		Fe spin population[b]		E spin population[b]	
	S = 1	S = 2	S = 1	S = 2	S = 1	S = 2	S = 1	S = 2	S = 1	S = 2
1 (O−$CF_3CO_2^-$)	1.86	1.85	0.51	0.41	0.69	0.65	1.51	3.16	0.70	0.57
2 (S−$CF_3CO_2^-$)	1.80	1.88	0.51	0.39	0.55	0.58	1.04	2.85	0.97	0.87
3 (N−$CF_3CO_2^-$)	1.93	2.08	0.39	0.27	0.39	0.45	0.51	2.74	1.46	1.08
4 (N−none)	1.79	1.90	0.44	0.35			0.46	2.89	1.52	0.94
5 (N−CH_3CN)	1.70	1.93	0.39	0.28	0.30	0.23	0.44	2.64	1.50	1.18
6 (N−N_3^-)	1.80	1.96	0.38	0.27	0.27	0.33	0.51	2.72	1.44	1.09
7 (N−Cl^-)	1.61	1.77	0.38	0.27	0.22	0.29	0.48	2.75	1.49	1.06
8 (N−NC^-)	1.73	1.93	0.37	0.26	0.40	0.40	0.48	2.68	1.47	1.14
9 (N−SR^-)	1.61	1.80	0.36	0.26	0.48	0.51	0.53	2.70	1.42	1.11

[a]Bond orders from Mayer analysis. [b]Values from Mulliken analysis.

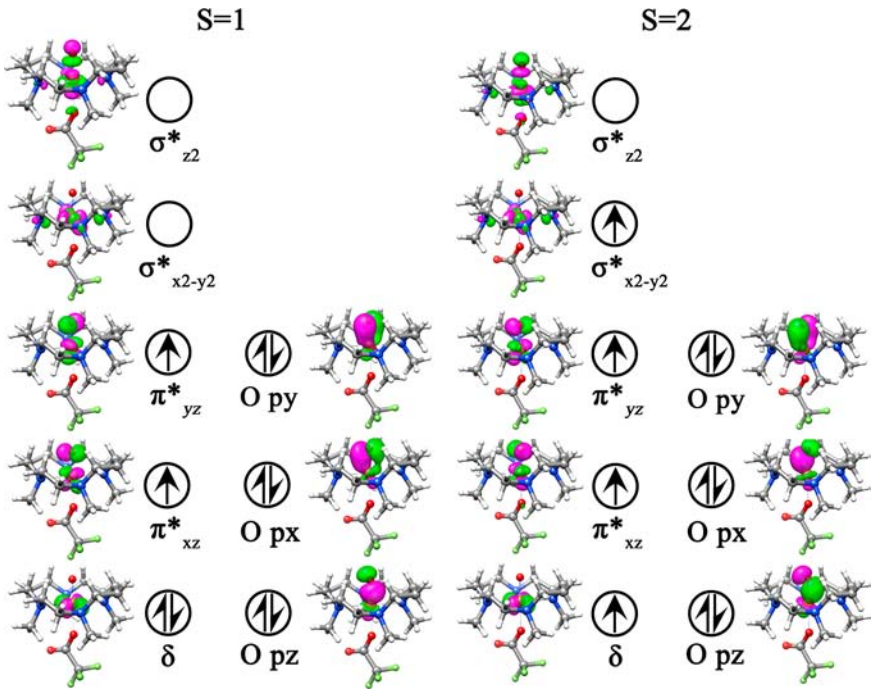

Figure 2. Orbital occupancy diagram for the triplet (S = 1) and quintet (S = 2) states of case **1** ($[Fe^{IV}$═O(TMC)$(CF_3CO_2)]^+$).

2, and **3** in the triplet state, respectively. The Fe═O bond length in the high spin state is not different from that in the ground state, while both the Fe═S and Fe═N bond lengths in the triplet spin state are slightly longer by 0.03 Å than those in the quintet spin state. Similar to those previously found in several nonheme iron(IV)−oxo species,[18a,33a,41a,46] the equatorial Fe−N distances in **1**, **2**, and **3** are expanded by 0.09, 0.10, and 0.11 Å in the high spin state relative to the S = 1 state, respectively. This geometric difference is attributed to the occupation of the $\sigma^*_{x^2-y^2}$ orbital, which is strongly antibonding with respect to the equatorial Fe−N bonds. Another comparison of the structures in **1**, **2**, and **3** is that the axial Fe−L_{ax} distances trans to the oxo, sulfide, and nitrido groups in the low spin state are slightly longer than those in the high spin state. The axial Fe−L_{ax} distances are 2.05 Å in case **1**, 2.07 Å in case **2**, vs 2.28 Å in case **3** in the triplet state, suggesting that the nitrido ligand exerts the strongest trans influence among these three ligands, so it is as observed in the high spin state where the longer Fe−L_{ax} length in case **3** exerts a more of a trans influence than those in **1** and **2**.

Table 1 lists important information from the electronic structure calculations with the B3LYP functional. The calculated bond orders of 1.86, 1.80, and 1.93 in cases **1**, **2**, and **3** for the triplet state are close to the ideal value of 2.00 for oxidation state IV, in particular in the Fe^{IV}═N species due to the less significant L_{ax}═Fe═N three-center bonding. In both the triplet and quintet states, the stronger Fe═N bond occurs at the expense of equatorial Fe−N bonding to the TMC ligands. The average Fe−N bond orders (0.39 in S = 1 and 0.27 in S = 2) in case **3** are significantly less than the corresponding Fe−O/S bond orders of both 0.51 in the triplet state as well as 0.39 and 0.41 in the quintet state of cases **1** and **2**. Another interesting result of the bond order analysis presented in Table 1 is the trend in Fe−L_{ax} bond orders trans to the Fe═E bond. The largest bond order (0.69 in S = 1 and 0.65 in S = 2) has been observed in case **1**, while the values of 0.55 and 0.58 in the triplet and quintet states are obtained in case **2**. The smallest bond order is calculated for case **3** (0.39 in S = 1 and 0.45 in S = 2). Obviously, the nitrido ligand exerts a stronger trans influence than both the oxo and sulfide ligands.

Since some unpaired spin density in the paramagnetic **3** typically delocalizes onto the multiply bonded E atom, the distributions of spin for S = 1 and S = 2 in the analogous iron(IV)−oxo, −sulfido, and −nitrido are comparable. The iron

dx.doi.org/10.1021/ic302766f | Inorg. Chem. 2013, 52, 2684−2696

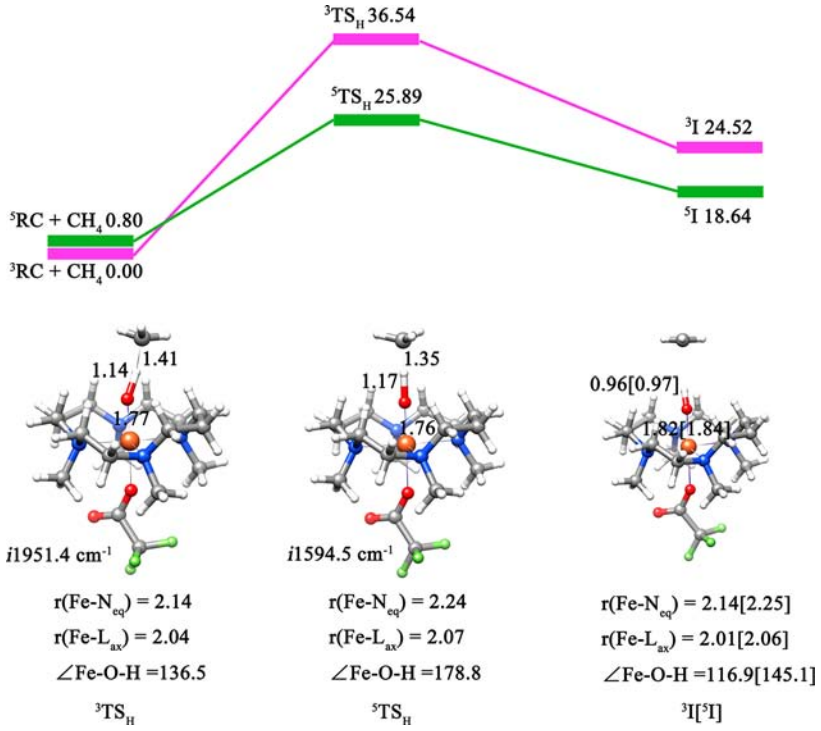

Figure 3. Calculated potential-energy surface corresponding to the methane hydroxylation by case **1** ([Fe^{IV}═O(TMC)(CF$_3$CO$_2$)]$^+$). All energies are relative to isolated reactants in the triplet spin state. Bond lengths are given in Ångstroms, and the imaginary frequency in the transition state is in wave numbers.

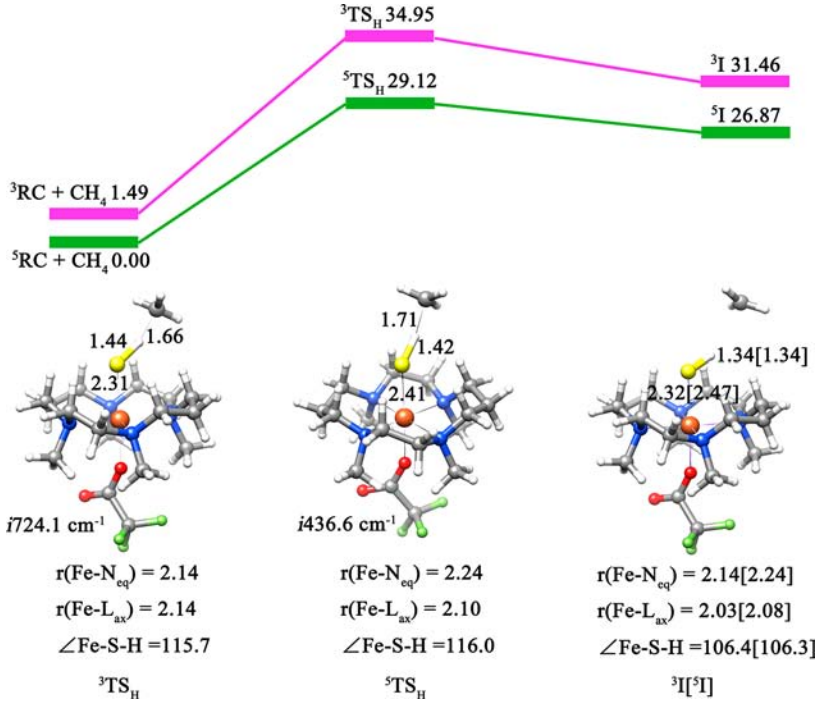

Figure 4. Calculated potential-energy surface corresponding to the methane hydroxylation by case **2** ([Fe^{IV}═S(TMC)(CF$_3$CO$_2$)]$^+$). All energies are relative to isolated reactants in the quintet spin state. Bond lengths are given in Ångstroms, and the imaginary frequency in the transition state is in wave numbers.

atom in case **1** carries only some of the spin population (1.51 and 3.16 for S = 1 and S = 2, respectively) with the remainder essentially locating on the oxo ligand, in contrast to the iron spin population value of 1.04 and 2.85 for the triplet and quintet states in case **2**, while 0.97 and 0.87 for the corresponding sulfide ligands. Differently, in case **3**, the spin population for the S = 1 state is more localized on the N atom than are the iron(IV)−oxo and −sulfido compounds, indicating the larger covalency of Fe═N as compared to Fe═O and Fe═S.

dx.doi.org/10.1021/ic302766f | *Inorg. Chem.* 2013, 52, 2684−2696

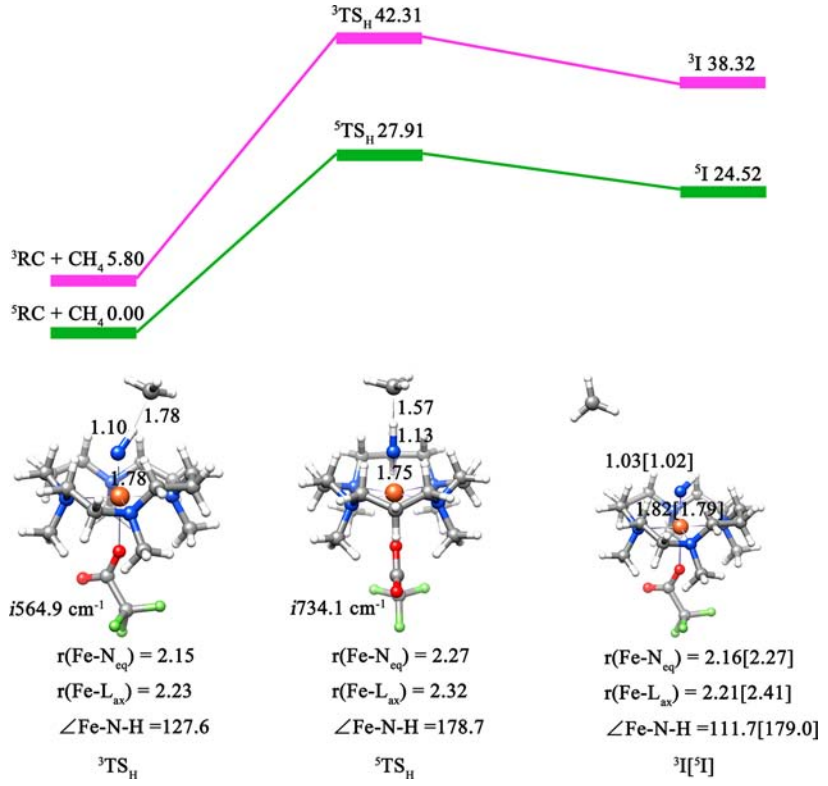

Figure 5. Calculated potential-energy surface corresponding to the methane hydroxylation by case **3** ([Fe^{IV}═N(TMC)(CF$_3$CO$_2$)]). All energies are relative to isolated reactants in the quintet spin state. Bond lengths are given in Ångstroms, and the imaginary frequency in the transition state is in wave numbers.

Shown in Figure 2 are the electron configurations corresponding to the low-spin and high-spin states of case **1** (same electron configurations as case **1** are observed in cases **2** and **3**). This d block spreads into the two typical patterns of distorted octahedral with the overlap of Fe 3d and O/S/N 2p orbitals. One group consists of bonding/antibonding pairs with π symmetry (O/S/N-$p_{x/y}$: $d_{xz/yz}+p_{x/y}$; Fe-$\pi^*_{xz/yz}$: $d_{xz/yz}-p_{x/y}$) and σ symmetry (O/S/N-p_z: $d_{z^2}+p_z$; Fe-$\sigma^*_{z^2}$: $d_{z^2}-p_z$), respectively. The other group involves the δ and $\sigma_{x^2-y^2}$* orbitals with δ symmetry. All of the considered Fe^{IV}(E) complexes exhibit two electronic states, the triplet state with a $(\delta)^2$ $(\pi_{xz}^*)^1$ $(\pi_{yz}^*)^1$ electron configuration, and the quintet state possessing a $(\delta)^1$ $(\pi_{xz}^*)^1$ $(\pi_{yz}^*)^1$ $(\sigma_{x^2-y^2}^*)^1$. A triplet ground spin state is computed for case **1**, which agrees with the experimental results,[12e] whereas all the other functionals used by us predict a quintet ground state for cases **2** and **3** (Table S1, Supporting Information). Note that among the energetic gaps between the S = 1 and S = 2 states in the cases **1**−**3**, case **3** has larger energetic gap than cases **1** and **2**.

3.2. H-Abstraction Reactions from CH$_4$ by [Fe^{IV}═N(TMC)(CF$_3$CO$_2$)] and [Fe^{IV}═E(TMC)(CF$_3$CO$_2$)]$^+$ (E = O^{2-} and S^{2-}). In order to get a reliable measurement of the relative potency of **3** as an oxidant, studies on the reactivity of **1** and **2** under the same conditions with respect to H-atom abstraction reaction are performed. Figures 3−5 show the calculated energy profiles for all the reagents **1**−**3** reacting with CH$_4$, involving the optimized geometries and the corresponding imaginary frequencies of the triplet and quintet transition states of the reagents **1**−**3**.

As usually established for the hydrogen-abstraction reaction, in the mechanism for **1** the reactants form a reactant cluster (^{3,5}**RC**), followed by a TS (^{3,5}**TS$_H$**) for hydrogen abstraction that leads to an intermediate (^{3,5}**I**).[3,33a,47,48] Figure 3 shows the calculated energy profile for case **1** reacting with CH$_4$. Inspection of Figure 3 reveals that case **1** has a triplet ground state (S = 1) and a low-lying excited-quintet state (S = 2). On the triplet and quintet surfaces, the free energy barriers at the B3LYP/B2//B1 level were found to be 37 and 26 kcal mol^{-1} relative to the separated reactants, respectively. However, as addressed recently by Lonsdale et al.[49] and found herein too, inclusion of dispersion correction lowers the H-abstraction barriers by about 5 to 32 kcal mol^{-1} for the S = 1 and 21 kcal mol^{-1} for the S = 2 spin states (Table S3, Supporting Information). As the quintet state starts as an excited state, albeit of low energy, and cuts through the larger triplet state barrier, here, a two-state reactivity (TSR) mechanism is a plausible scenario for C−H bond activation by case **1**, which is similar to the nonheme iron(IV)−oxo complexes previously reported.[33a,b]

For **2**, the methane hydroxylation starts with a hydrogen-atom abstraction via transition state **TS$_H$** to yield an intermediate. The reaction profile for methane hydroxylation by case **2** is displayed in Figure 4. As shown, the lowest lying barrier for C−H bond hydroxylation here is on the quintet spin state surface, which is 6 kcal mol^{-1} lower in energy than that for the triplet spin state surface. The dispersion correction also decreases the reaction barriers of case **2**, which highlights the very significant effect of van der Waals interaction (Table S3, Supporting Information).[44,49−51] As such, for case **2** the reaction starts with a quintet state reactant and then primarily proceeds on energetically low-lying quintet-state energy surface.

The mechanism for **3** is analogous to that by iron(IV)−oxo and iron(IV)−sulfido complexes,[3,33a,47,48] which has little precedent in metal nitride chemistry. This mechanism first

dx.doi.org/10.1021/ic302766f | Inorg. Chem. 2013, 52, 2684−2696

requires a direct attack on the hydrogen atom of the methane to form [Fe^{III}═NH(TMC)(CF_3CO_2)]. Figure 5 illustrates the energy profile for hydroxylation of CH_4 by case **3**. At the **RC** state, the quintet state is energetically more favorable than the triplet state by 6 kcal mol^{-1} at the B3LYP/B2//B1 level. Therefore, it is proposed that the reaction starts exclusively at the quintet state. The barrier at the B3LYP/B2//B1 level in the quintet state is calculated to be 28 kcal mol^{-1}, and that for the triplet state is 42 kcal mol^{-1}. B3LYP+VDW shown in Table S3 in the Supporting Information lowers these barriers to 23 and 34 kcal mol^{-1} on the quintet and triplet surfaces, respectively. This means that the reaction for case **3** will proceed faster on the quintet spin state surface than the triplet one. Consequently, the quintet state in case **3** will dominate the reactivity, that is, single-state reactivity on the quintet surface.

In summary, on the basis of the above analysis one may anticipate a few trends. First, in addition to B3LYP, all the B3LYP-G, B3LYP+VDW, and PBE0 uniformly show that the ^{5}**TS**$_H$ is the lowest transition state for **1**−**3** (Tables S2 and S3, Supporting Information). The heightened reactivity of the S = 2 state in cases **1**−**3** toward C−H bond activation can be nicely explained by exchange-enhanced reactivity, similarly to the nonheme iron(IV)−oxo species studied computationally and experimentally.[22,33a,52] Second, in the reactivities comparisons, on the S = 1 surface, all the functionals uniformly exhibit that the iron(IV)−oxo and −sulfido species have similar reactivities, both of which are reactive relative to iron(IV)−nitrido complex. By contrast, the reactivity in the quintet state displays a decrease order as the iron ion gets ligated by O^{2-}, N^{3-}, and S^{2-}, albeit of the close efficiency in hydroxylating C−H bond of methane. Apart from the novel iron(IV)−nitrido complex **3** first discussed here, our computational results and reactivity trends are in perfect agreement with previous studies of hydrogen-atom abstraction reaction catalyzed by the iron(IV)−oxo and iron(IV)−sulfido species.[34]

In order to gain a greater understanding of the preference of the higher reactivity of S = 2 state relative to the S = 1 state, we discuss now the reactivities of the triplet and quintet states using the simplified orbital diagram in Scheme 2 that follows the electronic reorganization during the H abstraction. As reported previously,[21b,33a] C−H bond cleavage is induced by a shift of an electron from the C−H α/β orbital into a corresponding low lying empty molecular orbital of the iron(IV)−oxo species, for which the Fe-$\sigma^*_{z^2}$ (α) and Fe-$\pi^*_{xz/yz}$ (β) orbitals serve as electron acceptors, namely σ-mechanism and π-mechanism, respectively. As shown in Figure 6 a β electron transfers to the Fe-$\pi^*_{xz/yz}$ (β) orbital and thus creates the ^{3}**I** intermediates with Fe^{III} centers and $C^{\bullet}$ radical cation, which can be viewed as the triplet π-mechanism discussed above. An Fe−O−H angle for the π-mechanism is close to 120° as found in ^{3}**TS**, which results from the balance between the orbital interaction and the Pauli repulsion.[22,33a] Indeed, a sideways trajectory with Fe−O−H angles of 136.5°, 115.7°, and 127.6° on the triplet transition state were found in cases **1**, **2**, and **3**.

As shown in Figure 7, in contrast to the π-mechanism, for ^{5}**TS**$_H$ of case **1**, **2**, and **3**, the H-abstraction reaction during S = 2 is identified as an established σ-mechanism in which the electron is shifted to Fe-$\sigma^*_{z^2}$ orbital that is aligned along the Fe−O axial. The geometry parameters are in line with the reaction mechanisms, that is, an Fe−O−H angle of 178.8° for **1** and 178.7° for **3** in ^{5}**TS**. Nevertheless, the Fe−S−H angle of 116.0° computed in $^{5\sigma}$**TS** of case **2** presents a significant

Scheme 2. Electron Shifts Diagrams for Hydrogen-Abstraction Reactions from CH_4 by All the Complexes in (a) S = 1, σ, (b) S = 1, π, and (c) S = 2 Spin States

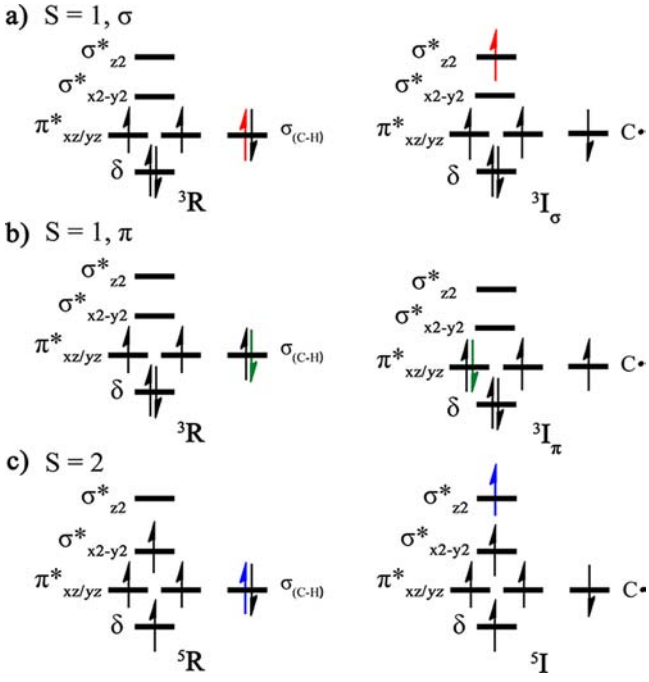

deviation from ideal linear geometry, which may be explained by the fact that the reaction for case **2** has higher barrier in the quintet state compared to cases **1** and **3**, and thus, the reaction involves rather late transition state.

The geometric features of the optimized transition states, here too, are in accordance with the nature of the electron shifts as well as the general reactivity patterns of the Fe-bound ligands' reagents. The geometries of the triplet and quintet transition states of the reagents **1**−**3** are displayed in Figures 3−5. One of the most prominent changes in ^{3,5}**TS** is the elongation of the Fe═E bond in comparison with that in the reactant. Case **3** exhibits a slight lengthening of the Fe═N bond by 0.07 Å for S = 1 and 0.08 Å for S = 2 relative to those in case **1** (0.15 Å for S = 1 vs 0.14 Å for S = 2) and case **2** (0.20 Å for S = 1 vs 0.34 Å for S = 2). Furthermore, close inspection of the cleavage of a C−H bond and the formation of an O/N−H bond indicates that ^{5}**TS** species in cases **1** and **3** are somewhat earlier transition states compared to the triplet one, which is consistent with the higher reactivity of the quintet state. Note that the equatorial Fe−N distances of the transition states are greatly determined by the spin state. For the complexes **1**, **2**, and **3**, the averaged Fe−N distances in ^{5}**TS** are found to be 2.24, 2.24, and 2.27 Å, which are longer than those of 2.14, 2.14, and 2.15 Å in ^{3}**TS**, respectively. This geometric difference arises from the occupation of the $\sigma_{x^2-y^2}$* orbital only in the quintet state, rather than in the triplet state. As such, we may conclude that the spin-dependent equatorial Fe−N bond is common not only to the nonheme iron(IV)−oxo oxidants, but also to the iron(IV)−sulfido and iron(IV)−nitrido complexes used herein, wherever the two transition states could be located.

Subsequently, to explore the oxidative power of the Fe^{IV}(E) complexes, we investigated the correlation between the barrier heights of C−H hydroxylation with cases **1**−**3** and the bond dissociation energies (BDEs) of E−H bond in the

dx.doi.org/10.1021/ic302766f | Inorg. Chem. 2013, 52, 2684−2696

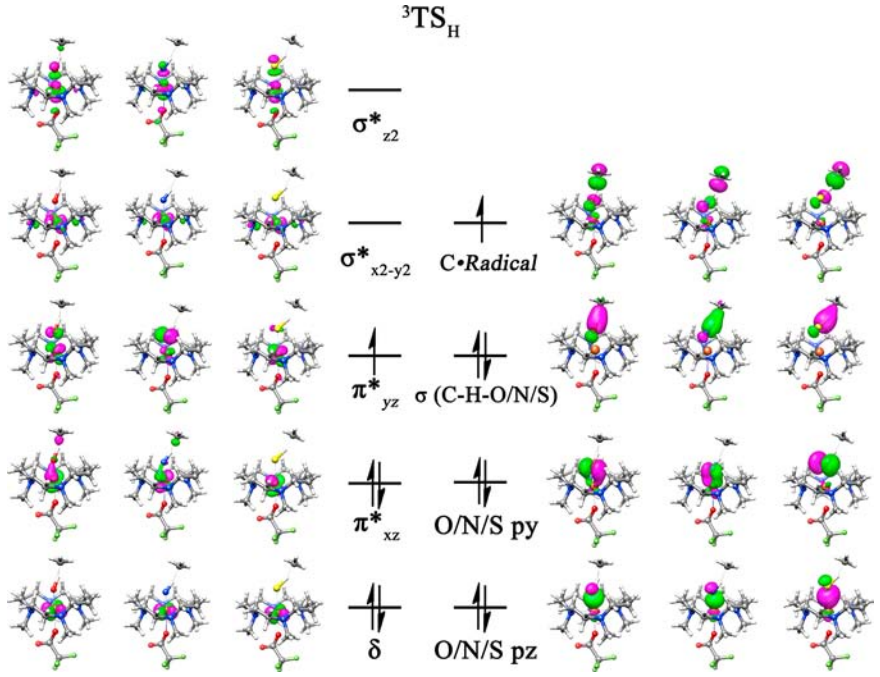

Figure 6. Schematic MO diagrams of ^3TS_H for cases **1**, **2**, and **3**.

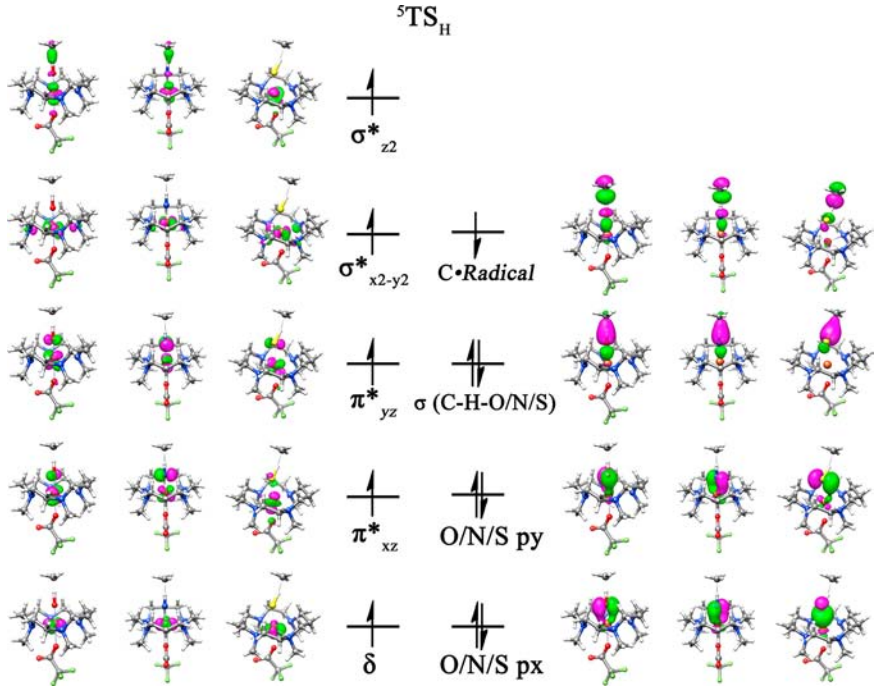

Figure 7. Schematic MO diagrams of ^5TS_H for cases **1**, **2**, and **3**.

$TMCFe^{III}(E)-H$ species, as done before by Mayer,[53] Borovik et al.,[54] and their respective co-workers for the contribution on BDE(O−H) chemistry and its correlation with reaction rates. Table 2 summarizes the barriers of methane hydroxylation by the three oxidants **1**−**3** as well as the BDE values of each model (BDE_{OH}, BDE_{SH}, and BDE_{NH}). Figure 8 displays the calculated hydrogen abstraction barriers of methane as a function of $BDE_{OH/SH/NH}$ for the quintet spin state. The calculated BDE_{EH} values of cases **1**, **2**, and **3** are 91.0, 82.8, and 86.2 kcal mol^{-1}, respectively. Despite the somewhat different $BDE_{OH/SH/NH}$ values, it is seen that the largest BDE is for case **1**, the smallest is for case **2**, and the BDE_{NH} of case **3** is between that of cases **1** and **2**, which is in accord with the computed trend of the barriers and further reflects that the iron(IV)−nitrido complex is able to serve as oxidant candidates and have the oxidative power of hydroxylating C−H bond of methane as efficiently as the iron(IV)−oxo and −sulfido species.

3.3. Predict Reactivity Model for the Iron(IV)−Nitrido Complexes. *3.3.1. Properties of the $[Fe^{IV}{=}N(TMC)(L_{ax})]^{n+}$ Complexes.* Considering that the iron(IV)−nitrido complex $[Fe^{IV}{=}N(TMC)(CF_3CO_2)]$ has been found to be highly reactive and capable of activating the C−H bond of methane, in

dx.doi.org/10.1021/ic302766f | Inorg. Chem. 2013, 52, 2684−2696

Table 2. DFT Calculation Hydrogen Abstraction Barriers for the Quintet State by All the Oxidants and the Calculated Values of BDE_{EH}, RE_{FeEH}

oxidant	BDE_{EH}	RE_{FeEH}	^5TS_H[a]
1 (O−$CF_3CO_2^-$)	91.0	−19.6	25.9
2 (S−$CF_3CO_2^-$)	82.8	−2.9	29.1
3 (N−$CF_3CO_2^-$)	86.2	−4.9	27.9
4 (N−none)	96.0	−7.7	20.7
5 (N−CH_3CN)	88.7	−6.3	27.2
6 (N−N_3^-)	86.2	−4.7	27.7
7 (N−Cl^-)	85.2	−4.2	28.0
8 (N−NC^-)	85.6	−4.8	28.5
9 (N−SR^-)	85.5	−4.3	28.2

[a]All values are in kcal mol^{-1} and calculated at B3LYP/B2//B3LYP/B1.

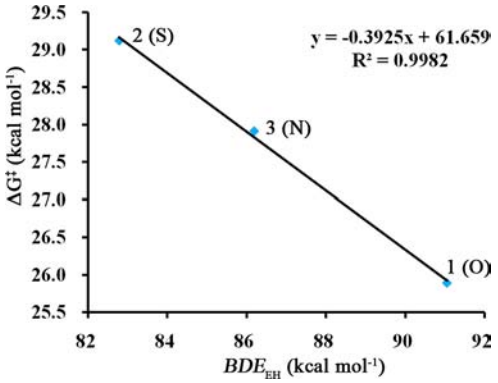

Figure 8. Correlation between the height of the barrier (^5TS_H) for methane hydroxylation and BDE_{EH} value. The complexes tested were $[Fe^{IV}{=}E(TMC)(CF_3CO_2)]^{+/0}$: E = O^{2-}, S^{2-}, and N^{3-}. All values were in kcal mol^{-1} and calculated with B3LYP/B2//B3LYP/B1.

a further set of calculation, we therefore searched for the more iron(IV)−nitrido complexes and elaborated the axial ligand effect on the C−H hydroxylation using the extensive iron(IV)−nitrido systems with variable axial ligands (L_{ax}): $[Fe^{IV}{=}N(TMC)(L_{ax})]^{n+}$ (L_{ax} = none, CH_3CN, $CF_3CO_2^-$, N_3^-, Cl^-, NC^-, and SR^-). As simple notations for the iron(IV)−nitrido reagents, we shall use the symbol **N−L_{ax}**, where L_{ax} indicates the axial ligand.

Figure 1 illustrates the optimized geometries of the oxidants $[Fe^{IV}{=}N(TMC)(L_{ax})]^{n+}$ (L_{ax} = none, CH_3CN, $CF_3CO_2^-$, N_3^-, Cl^-, NC^-, and SR^-) in the two states of triplet and quintet, whereas the optimized transition state structures are given in Figure 9. The geometric data of the iron(IV)−nitrido species in Figure 1 agree well with the discussion above, that is, a fairly constant Fe=N bond length. By contrast, the Fe−N_{eq} bonds undergo lengthening in the quintet state, in accord with the occupation of the $\sigma^*_{x^2-y^2}$ orbital (Figure 2). Additionally, the amount of the spin population on the N atom increases as the electron releasing power of the axial ligand enhances. It is seen that these oxidants are characterized by a quintet ground state, $(\delta)^1$ $(\pi^*_{xz})^1$ $(\pi^*_{yz})^1$ $(\sigma^*_{x^2-y^2})^1$ $(\sigma^*_{z^2})^0$, with a triplet state of a $(\delta)^2$ $(\pi^*_{xz})^1$ $(\pi^*_{yz})^1$ $(\sigma^*_{x^2-y^2})^0$ $(\sigma^*_{z^2})^0$ electron configuration lying above energetically. All the functionals uniformly give the same spin-state ordering (Table S1, Supporting Information), which enables us to confidently assign the ground state of the oxidants as a quintet state.

According to the calculations, the triplet−quintet-state gaps increasing in the order of **N−none** < **N−CH_3CN** < **N−$CF_3CO_2^-$** are obtained: the **N−none** case being devoid of an axial ligand displays the smallest gap, while the **N−$CF_3CO_2^-$** case, where the axial ligand possesses a negative charge, presents the largest gap. We start with considering the main factors that may have contributed to the state ordering. First, the binding strength of the equatorial Fe−N bonds is stronger in **N−none** compared to **N−CH_3CN** and **N−$CF_3CO_2^-$**, as reflected by the shorter Fe−N_{eq} bonds and larger bond orders (Table 1). The greater antibonding interactions between the $\sigma^*_{x^2-y^2}$ orbital and the equatorial TMC ligand lead to the higher energy of the $\sigma^*_{x^2-y^2}$ orbital, and therefore the triplet−quintet-state gap is smaller in **N−none** relative to **N−CH_3CN** and **N−$CF_3CO_2^-$**. The other one impacting the energy gap is the electron−electron repulsion between the electrons of the axial ligand and the electron pair in the δ orbital in the triplet state. As the electron−electron repulsion of the axial ligand with the electron pair in δ orbital of iron gets stronger, an electron in the δ orbital can be excited to the $\sigma^*_{x^2-y^2}$ orbital more easily, which would further stabilize the quintet state. In our system, the series with different axial ligands show apparent signs for the electron−electron repulsion with the axial ligand. For example, the **N−none** case without an axial ligand exhibits relatively close energy for the triplet and quintet states, while the **N−$CF_3CO_2^-$** case, where the axial ligand possesses a negative charge, displays an enlarged gap. Taken together, the present analysis implies that, for the $[Fe^{IV}{=}N(TMC)(L_{ax})]^{n+}$ species in the H-atom abstraction, the triplet−quintet energy gap increases as the electron-donating capabilities of the axial ligands strengthen.

Interestingly, a reverse trend of the triplet−quintet gap has been observed in the previous investigation on the hydrogen abstraction reactions of 9,10-dihydroanthracene in the $[Fe^{IV}{=}O(TMC)(L_{ax})]^{n+}$ complexes (L_{ax} = $CF_3CO_2^-$, CH_3CN, and none).[33a] These behaviors between the $[Fe^{IV}{=}N(TMC)(L_{ax})]^{n+}$ and $[Fe^{IV}{=}O(TMC)(L_{ax})]^{n+}$ complexes arise, however, simply from the difference in their ground states: quintet for $[Fe^{IV}{=}N(TMC)(L_{ax})]^{n+}$, whereas triplet for $[Fe^{IV}{=}O(TMC)(L_{ax})]^{n+}$. Clearly, if S = 2 is the ground state, to lower its energy means to increase the gap; in contrast, if S = 1 is the ground state, lowering the energy of the quintet state means decreasing the gap. Therefore, it seems that the effect of axial ligand (L_{ax}) is fundamentally the same for $[Fe^{IV}{=}N(TMC)(L_{ax})]^{n+}$ as for $[Fe^{IV}{=}O(TMC)(L_{ax})]^{n+}$ complexes, i.e., enhancing the stabilization of the quintet state with respect to the triplet state in the series L_{ax} = none, CH_3CN, $CF_3CO_2^-$.

3.3.2. H-Abstraction Reactions from CH_4 by a Series of the $[Fe^{IV}{=}N(TMC)(L_{ax})]^{n+}$ Complexes. Figures S1−S6 illustrate the generic energy profiles for the $[Fe^{IV}{=}N(TMC)(L_{ax})]^{n+}$ oxidants with methane, in which all the functionals have the same spin-state ordering of the energy. All the C−H activation reactions by the $[Fe^{IV}{=}N(TMC)(L_{ax})]^{n+}$ systems with CH_4 start with the quintet ground state, which benefits from the exchange-enhanced stabilization, as discussed above, and it is the lowest profile throughout.

As the simplified orbital diagrams in Scheme 2 that shows the evolution of d-orbital occupancy during the H-abstraction, on the triplet state surface, the Fe-$\pi^*_{xz/yz}$ orbital of all the iron(IV)−nitrido complexes acts as the electron acceptor, except for **N−none**, whereas the Fe-$\sigma^*_{z^2}$ orbital accepts electron from the substrate on the quintet state. The geometric features of the optimized transition states for the iron(IV)−nitrido complexes are in line with the nature of the electron shifts in Figures S7−S12. Thus, as further shown in Figure 9,

dx.doi.org/10.1021/ic302766f | Inorg. Chem. 2013, 52, 2684−2696

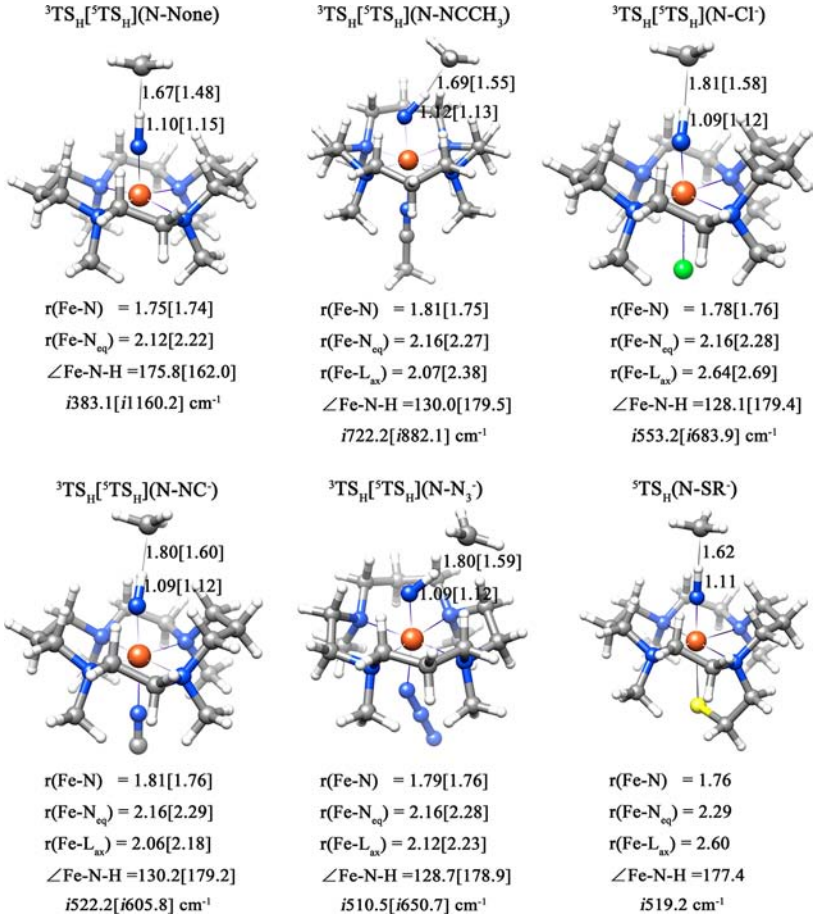

Figure 9. Optimized geometries of triplet and quintet transition states for H abstraction. Bond lengths are in Ångstroms, angles in degrees, and the imaginary frequency in the transition state is in wave numbers. For the triplet and quintet transition states structures of cases **1**−**3**, see Figures 3−5.

^{3}**TS** is characterized by a bent sideways trajectory, which reflects the compromise between the orbital interactions and Pauli repulsion.[22,33a] By contrast, ^{5}**TS** requires an essentially linear attack. The unusual reaction pattern of **N**−**none** will be analyzed below.

As inferred from the group spin densities and charges collected in Tables S3 and S4 in the Supporting Information, all the transition states and intermediates in the substrates considered have significant radical characters. For example, when L_{ax} = Cl^-, the intermediate is radical in character with group spin densities of ρ_{CH3} = −0.98 (1.00) for ^{5}**I**$_{Cl}$ (^{3}**I**$_{Cl}$), while the charge on this group is Q_{CH3} = −0.02 (0.00). Similar observations have been made for the hydrogen-atom transfer from ethylbenzene hydroxylation by $[Fe^{IV}{=}O(TMC)(Cl)]^{+}$[55] and $[Fe^{IV}{=}O(Por{+}\cdot)(Cl)]$,[56] as reported recently. However, in sharp contrast to the hydride transfer with ethylbenzene in the aliphatic hydroxylation of the ethylbenzene with $[Fe^{IV}{=}O(TMC)(NCCH_3)]^{2+}$,[55] the acetonitrile axial ligand in $[Fe^{IV}{=}N(TMC)(L_{ax})]^{n+}$ here still gives a radical intermediate.

Now we check the influence of the axial ligand carrying different charges on the reactivity by examining the systems $[Fe^{IV}{=}N(TMC)(L_{ax})]^{n+}$, whose axial ligand is substituted with neutral ligand CH_3CN and negatively charged ligands $CF_3CO_2^-$, Cl^-, NC^-, N_3^-, and SR^-, respectively. As the energy profile suggests, the CH_3CN-substituted complex features a lower barrier than the negatively charged ligands in both the triplet and quintet states. Therefore, we can conclude that the axial ligand carrying more negative charge could weaken the ability of a $[Fe^{IV}{=}N(TMC)(L_{ax})]^{n+}$ complex to promote C−H bond breaking.

Furthermore, different electron pushing capabilities of the negatively charged axial ligand has been found to impact the H-abstraction barriers. For all the computed barriers of the iron(IV)−nitrido series, those obtained from the lowest quintet state of $[Fe^{IV}{=}N(TMC)(L_{ax})]^{n+}$ also represent the observed axial ligand effect, showing a decrease of the reactivity in the following order of the axial ligand L_{ax}: N_3^- > $CF_3CO_2^-$ > Cl^- > SR^- > NC^-. As will be analyzed subsequently, this can be explained in terms of the destabilization effect of the Fe-$\sigma^*_{z^2}$ orbital by the anionic axial ligand.[50,52b] It is seen from Scheme 2 that in S = 2 an α-spin electron is shifted to the Fe-$\sigma^*_{z^2}$ orbital, which has strong L_{ax}−Fe antibonding character.[15a,20b,33a,b,50,52] When the electron-donating ability of the axial ligand (L_{ax}) is strong (such as NC^- and SR^-), the quintet barriers are high, which, on the contrary, decrease when the electron-donating ability of the axial ligand is weak. As such, the catalytic properties of the $[Fe^{IV}{=}N(TMC)(L_{ax})]^{n+}$ systems can be fine-tuned by varying the electron pushing abilities of the axial ligands.

We have verified that a stronger σ-donating axial ligand in the $[Fe^{IV}{=}N(TMC)(L_{ax})]^{n+}$ systems could weaken the reactivity of methane C−H activation reactions, and the barriers on the quintet surface follow the electrophilicity of the iron(IV)−nitrido reagents: the barrier is lower in the case of **N**−**CH$_3$CN** than those with the charge −1. It is thus natural to expect that a iron(IV)−nitrido system with no axial ligand might yield an

dx.doi.org/10.1021/ic302766f | *Inorg. Chem.* 2013, 52, 2684−2696

even higher reactivity than that with neutral CH_3CN ligand. For that reason we studied the compound $[Fe^{IV}{=}N(TMC)(None)]^+$, in which the axial ligand is removed. Figure S1 displays the corresponding reaction profile of **N−none** with CH_4. The reaction starts on the quintet ground state and then proceeds along the energetically low-lying quintet state reaction pathway. Different from the triplet π-mechanism in the other iron(IV)−nitrido cases discussed above, **N−none** proceeds through a nonclassical σ-mechanism in which the substrate approaches the oxidant from the top due to an α-spin electron transfer from the C−H bond into Fe-$\sigma^*_{z^2}$ antibonding orbital that is located along the Fe−O axis (Figure S7), as do the features in the corresponding ^{5}**TS$_H$** with a nearly collinear Fe−O−H arrangement. Compared with the barrier on the triplet surface, the reagent **N−none** has by far the lowest barrier among all the $[Fe^{IV}{=}N(TMC)(L_{ax})]^{n+}$ reagents, even following the triplet σ-mechanism.

Accordingly, the reactivity of the $[Fe^{IV}{=}N(TMC)(L_{ax})]^{n+}$ oxidants for the H-abstraction reaction was obtained in the decreased order of L_{ax} at the B3LYP level: none > CH_3CN > N_3^- > $CF_3CO_2^-$ > Cl^- > SR^- > NC^-, respectively. A similar trend to that of B3LYP has also been observed when employing the other functionals, i.e., B3LYP-G, B3LYP+VDW, and PBE0. This result is consistent with the experimental observation by Rohde and Que that $[Fe^{IV}{=}O(TMC)(L_{ax})]^{2+}$ with the axial CH_3CN ligand is favored in reactivity over the axial carboxylate ligand $CF_3CO_2^-$,[12e] as well as the finding that the acetonitrile axial ligand in $[Fe^{IV}{=}O(TMC)(L_{ax})]^{n+}$ is orders of magnitude more reactive than a chloride axial ligand, which was interpreted by the fact that the metal−ligand interactions influence the orbital energies and, as a consequence, the electron affinities and hydrogen atom abstraction abilities.[55] However, some synthetic iron and manganese oxo complexes have utilized electron-rich axial ligands to enhance their reactivity toward H-atom abstraction, for which multistate reactivity has been suggested.[32c,33b,57]

Previous computational studies on the substrate epoxidation reaction using a series of heme and nonheme iron(IV)−oxo models with varying axial ligands reported a linear relationship between the barrier height and the BDE_{OH} value of the oxidant, whereby BDE_{OH} is a reasonable evaluation for the C−O bond formation energy.[58] Consequently, to mimic the formation of a H−N bond in substrate-hydroxylation mediated by the iron(IV)−nitrido complex, we investigated the correlation between the height of the barrier and the BDE_{OH} value. The bond dissociation energies (BDEs) of N−H bond in the $TMCL_{ax}Fe^{III}(N)$−H species for the preferred quintet channel have been computed, and the correlation between the calculated hydrogen abstraction barriers and BDE_{NH} is presented in Figure 10. Although there is a bit of scatter in the data, the obtained correlation between barrier height and BDE_{NH} is reasonable and could well manifest the axial-ligand-effect on methane hydroxylation mediated by the iron(IV)−nitrido oxidants. Recent studies of H-abstraction reactions by a range of iron(IV)−oxo and manganese(V)−oxo corrolazine complexes showed a strong axial ligand effect on the barrier heights proportional to a dramatic change in the BDE_{OH} value of the oxidant, in agreement with the trend observed here.[47c,57] As follows from Figure 10, the hydrogen abstraction barriers decrease with the increase of the BDE_{NH} of the oxidants. For example, with BDE_{NH} progressively increasing among the representative ligands L_{ax} = none, CH_3CN, $CF_3CO_2^-$, successively, the reaction barriers decrease in the sequence

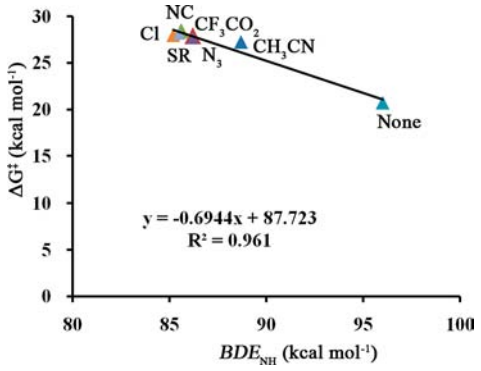

Figure 10. Correlation between the height of the barrier (^{5}**TS$_H$**) for methane hydroxylation and BDE_{NH} value. The complexes tested were $[Fe^{IV}{=}N(TMC)(L_{ax})]^{n+}$ with L_{ax} = none, CH_3CN, $CF_3CO_2^-$, N_3^-, Cl^-, NC^-, and SR^-. All values were in kcal mol^{-1} and calculated with B3LYP/B2//B3LYP/B1.

N−none > **N−CH_3CN** > **N−$CF_3CO_2^-$**. This implies that BDE_{NH} is a reasonably excellent representative of the axial ligand effect in C−H bond activation, and the formation of a H−N bond can be faithfully mimicked with the formation of a H−O bond.

4. CONCLUSIONS

A series of novel octahedral iron(IV)−nitrido complexes using the TMC ligand in the equatorial plane and one axial ligand trans to the nitrido have been theoretically constructed, where the ligand environment is used to mimic the similar ligand sphere as that in the mononuclear iron(IV)−oxo complex. On the basis of systematic density-functional theory calculations, we have presented a comparative study on the electronic properties and reactivities of iron(IV)−nitrido complexes regarding the iron(IV)−oxo and iron(IV)−sulfido counterparts, and further, the effect of axial ligands has also been elaborated.

The hydroxylation mechanism promoted by the iron(IV)−nitrido complexes herein establishes that one hydrogen atom is abstracted from the methane by the iron(IV)−nitrido species, leading to an $Fe^{III}(N)$−H moiety together with a carbon radical, similar to the cases by the iron(IV)−oxo and iron(IV)−sulfido compounds. DFT results reveal that, unlike the well-known iron(IV)−oxo species that tends to react on two-state reactivity surfaces in the H-abstraction reaction with the S = 1 ground state, the sampled iron(IV)−nitrido and iron(IV)−sulfido complexes are all in a stable S = 2 state, and their exchange-enhanced reactivity mediates the H-abstraction reactivity at much lower barriers than that of the S = 1 spin state, indicating that it may be the single-state reactivity that dominates on the high-spin quintet surface. Moreover, the relative reactivity of the different iron-based complexes in methane hydroxylation reaction demonstrates that the iron(IV)−nitrido species are capable of activating C−H bond of methane, which can exhibit potential reactivity abilities as good as the iron(IV)−oxo and −sulfido counterparts. Additionally, analysis of the axial ligand effect on methane hydroxylation by iron(IV)−nitrido oxidants reveals that the reactivity of iron(IV)−nitrido oxidants in the quintet state enhances as the electron-donating ability of the axial ligand weakens.

Note that, apart from the iron(IV)−oxo complex and its reactivity, no relevant experimental data have been obtained on the iron(IV)−sulfido and iron(IV)−nitrido complex. However,

dx.doi.org/10.1021/ic302766f | Inorg. Chem. 2013, 52, 2684−2696

the present calculations predict that the $Fe^{IV}N$ and $Fe^{IV}S$ species can compete in oxidation power with that of $Fe^{IV}O$, which may deliver promising potentials in discovering and devising novel catalysts containing these motifs.

■ ASSOCIATED CONTENT

Supporting Information

Tables with relative energies, spin densities, charge analysis, figures of potential energy surfaces, orbital occupancy evolution diagrams, and correlations between the height of the barrier and $BDE_{EH} - RE_{FeOH}$. This material is available free of charge via the Internet at http://pubs.acs.org.

■ AUTHOR INFORMATION

Corresponding Author

*E-mail: huiling@jlu.edu.cn (H.L.); huangxr@jlu.edu.cn. (X.H.).

Notes

The authors declare no competing financial interest.

■ ACKNOWLEDGMENTS

This work is supported by the National Basic Research Program of China (973 Program) (2012CB932800), National Natural Science Foundation of China (NSFC No. 21073075 and 21173097), Research Fund for the Doctoral Program of Higher Education of China (RFDP No. 20100061110046), and Fundamental Research Fund of Jilin University (No. 201003043).

■ REFERENCES

(1) (a) Green, M. T. *Curr. Opin. Chem. Biol.* **2009**, *13*, 84. (b) Meunier, B.; de Visser, S. P.; Shaik, S. *Chem. Rev.* **2004**, *104*, 3947. (c) Pitie, M.; Pratviel, G. *Chem. Rev.* **2010**, *110*, 1018. (d) Gunay, A.; Theopold, K. H. *Chem. Rev.* **2010**, *110*, 1060.

(2) (a) Ener, M. E.; Lee, Y.-T.; Winkler, J. R.; Gray, H. B.; Cheruzel, L. *Proc. Natl. Acad. Sci. U.S.A.* **2010**, *107*, 18783. (b) Kumar, D.; de Visser, S. P.; Shaik, S. *J. Am. Chem. Soc.* **2004**, *126*, 5072. (c) Kumar, D.; Tahsini, L.; de Visser, S. P.; Kang, H. Y.; Kim, S. J.; Nam, W. *J. Phys. Chem. A* **2009**, *113*, 11713.

(3) Ye, S. F.; Neese, F. *Curr. Opin. Chem. Biol.* **2009**, *13*, 89.

(4) Arndtsen, B. A.; Bergman, R. G.; Mobley, T. A.; Peterson, T. H. *Acc. Chem. Res.* **1995**, *28*, 154.

(5) Hohenberger, J.; Ray, K.; Meyer, K. *Nat. Commun.* **2012**, *3*, 720.

(6) (a) Feig, A. L.; Lippard, S. J. *Chem. Rev.* **1994**, *94*, 759. (b) Que, L., Jr.; Ho, R. Y. N. *Chem. Rev.* **1996**, *96*, 2607. (c) Wallar, B. J.; Lipscomb, J. D. *Chem. Rev.* **1996**, *96*, 2625. (d) Solomon, E. I.; Brunold, T. C.; Davis, M. I.; Kemsley, J. N.; Lee, S.-K.; Lehnert, N.; Neese, F.; Skulan, A. J.; Yang, Y.-S.; Zhou, J. *Chem. Rev.* **2000**, *100*, 235.

(7) (a) Bugg, T. D. H. *Tetrahedron* **2003**, *59*, 7075. (b) Denisov, I. G.; Makris, T. M.; Sligar, S. G.; Schlichting, I. *Chem. Rev.* **2005**, *105*, 2253. (c) Shaik, S.; Kumar, D.; de Visser, S. P.; Altun, A.; Thiel, W. *Chem. Rev.* **2005**, *105*, 2279.

(8) (a) Altun, A.; Shaik, S.; Thiel, W. *J. Am. Chem. Soc.* **2007**, *129*, 8978. (b) Schoneboom, J. C.; Neese, F.; Thiel, W. *J. Am. Chem. Soc.* **2005**, *127*, 5840. (c) Debrunner, P. G.; Dexter, A. F.; Schulz, C. E.; Xia, Y. M.; Hager, L. P. *Proc. Natl. Acad. Sci. U.S.A.* **1996**, *93*, 12791.

(9) (a) Rutter, R.; Valentine, M.; Hendrich, M. P.; Hager, L. P.; Debrunner, P. G. *Biochemistry* **1983**, *22*, 4769. (b) Rutter, R.; Hager, L. P.; Dhonau, H.; Hendrich, M.; Valentine, M.; Debrunner, P. *Biochemistry* **1984**, *23*, 6809. (c) Schulz, C. E.; Rutter, R.; Sage, J. T.; Debrunner, P. G.; Hager, L. P. *Biochemistry* **1984**, *23*, 4743. (d) de Visser, S. P.; Shaik, S.; Sharma, P. K.; Kumar, D.; Thiel, W. *J. Am. Chem. Soc.* **2003**, *125*, 15779.

(10) (a) Krebs, C.; Fujimori, D. G.; Walsh, C. T.; Bollinger, J. M., Jr. *Acc. Chem. Res.* **2007**, *40*, 484. (b) Pestovsky, O.; Stoian, S.; Bominaar, E. L.; Shan, X.; Münck, E.; Que, L., Jr.; Bakac, A. *Angew. Chem., Int. Ed.* **2005**, *44*, 6871. (c) England, J.; Guo, Y.; Farquhar, E. R.; Young, V. G., Jr.; Münck, E.; Que, L., Jr. *J. Am. Chem. Soc.* **2010**, *132*, 8635. (d) Lacy, D. C.; Gupta, R.; Stone, K. L.; Greaves, J.; Ziller, J. W.; Hendrich, M. P.; Borovik, A. S. *J. Am. Chem. Soc.* **2010**, *132*, 12188.

(11) (a) Que, L., Jr. *Acc. Chem. Res.* **2007**, *40*, 493. (b) Rohde, J.-U.; In, J. H.; Lim, M. H.; Brennessel, W. W.; Bukowski, M. R.; Stubna, A.; Münck, E.; Nam, W.; Que, L., Jr. *Science* **2003**, *299*, 1037.

(12) (a) Balland, W.; Charlot, M. F.; Banse, F.; Girerd, J. J.; Mattioli, T. A.; Bill, E.; Bartoli, J. F.; Battioni, P.; Mansuy, D. *Eur. J. Inorg. Chem.* **2004**, *2*, 301. (b) Berry, J. F.; Bill, E.; Bothe, E.; Weyhermüller, T.; Wieghardt, K. *J. Am. Chem. Soc.* **2005**, *127*, 11550. (c) Jensen, M. P.; Costas, M.; Ho, R. Y. N.; Kaizer, J.; Mairata, i.; Payeras, A.; Münck, E.; Que, L., Jr.; Rohde, J.-U.; Stubna, A. *J. Am. Chem. Soc.* **2005**, *127*, 10512. (d) Kaizer, J.; Klinker, E. J.; Oh, N. Y.; Rohde, J.-U.; Song, W. J.; Stubna, A.; Kim, J.; Münck, E.; Nam, W.; Que, L., Jr. *J. Am. Chem. Soc.* **2004**, *126*, 472. (e) Rohde, J.-U.; Que, L., Jr. *Angew. Chem., Int. Ed.* **2005**, *44*, 2255.

(13) (a) Costas, M.; Mehn, M. P.; Jensen, M. P.; Que, L., Jr. *Chem. Rev.* **2004**, *104*, 939. (b) Chakrabarty, S.; Austin, R. N.; Deng, D.; Groves, J. T.; Lipscomb, J. D. *J. Am. Chem. Soc.* **2007**, *129*, 3514. (c) Friedle, S.; Reisner, E.; Lippard, S. J. *Chem. Soc. Rev.* **2010**, *39*, 2768.

(14) (a) Fujii, H. *Coord. Chem. Rev.* **2002**, *226*, 51. (b) Groves, J. T. *J. Inorg. Biochem.* **2006**, *100*, 434. (c) Groves, J. T.; Haushalter, R. C.; Nakamura, M.; Nemo, T. E.; Evans, B. J. *J. Am. Chem. Soc.* **1981**, *103*, 2884. (d) Jung, C. *Biochim. Biophys. Acta* **2011**, *1814*, 46. (e) Tinberg, C. E.; Lippard, S. J. *Acc. Chem. Res.* **2011**, *44*, 280.

(15) (a) Decker, A.; Rohde, J.-U.; Klinker, E. J.; Wong, S. D.; Que, L., Jr.; Solomon, E. I. *J. Am. Chem. Soc.* **2007**, *129*, 15983. (b) Li, F.; Meier, K. K.; Cranswick, M. A.; Chakrabarti, M.; Van Heuvelen, K. M.; Münck, E.; Que, L., Jr. *J. Am. Chem. Soc.* **2011**, *133*, 7256. (c) Hirao, H.; Li, F.; Que, L., Jr.; Morokuma, K. *Inorg. Chem.* **2011**, *50*, 6637.

(16) (a) Seo, M. S.; Kim, N. H.; Cho, K.-B.; So, J. E.; Park, S. K.; Clemancey, M.; Garcia-Serres, R.; Latour, J.-M.; Shaik, S.; Nam, W. *Chem. Sci.* **2011**, *2*, 1039. (b) Nam, W. *Acc. Chem. Res.* **2007**, *40*, 465.

(17) Schöneboom, J. C.; Cohen, S.; Lin, H.; Shaik, S.; Thiel, W. *J. Am. Chem. Soc.* **2004**, *126*, 4017.

(18) (a) Kumar, D.; Hirao, H.; Que, L., Jr.; Shaik, S. *J. Am. Chem. Soc.* **2005**, *127*, 8026. (b) Shaik, S.; Kumar, D.; de Visser, S. P. *J. Am. Chem. Soc.* **2008**, *130*, 10128.

(19) Siegbahn, P. E. M.; Borowski, T. *Acc. Chem. Res.* **2006**, *39*, 729.

(20) (a) Ensing, B.; Buda, F.; Gribnau, M. C. M.; Baerends, E. J. *J. Am. Chem. Soc.* **2004**, *126*, 4355. (b) Michel, C.; Baerends, E. J. *Inorg. Chem.* **2009**, *48*, 3628.

(21) (a) de Visser, S. P. *J. Am. Chem. Soc.* **2006**, *128*, 9813. (b) de Visser, S. P. *J. Am. Chem. Soc.* **2006**, *128*, 15809.

(22) (a) Geng, C. Y.; Ye, S. F.; Neese, F. *Angew. Chem., Int. Ed.* **2010**, *49*, 5717. (b) Ye, S. F.; Neese, F. *Proc. Natl. Acad. Sci. U.S.A.* **2011**, *108*, 1228.

(23) (a) Einsle, O.; Tezcan, F. A.; Andrade, S. L. A.; Schmid, B.; Yoshida, M.; Howard, J. B.; Rees, D. C. *Science* **2002**, *297*, 1696. (b) Barney, B. M.; Lee, H.-I.; Dos Santos, P. C.; Hoffman, B. M.; Dean, D. R.; Seefeldt, L. C. *Dalton Trans.* **2006**, *19*, 2277. (c) Smith, J. M.; Subedi, D. *Dalton Trans.* **2012**, *41*, 1423.

(24) (a) Betley, T. A.; Peters, J. C. *J. Am. Chem. Soc.* **2004**, *126*, 6252. (b) Hendrich, M. P.; Genderson, W.; Behan, R. K.; Green, M. T.; Mehn, M. P.; Betley, T. A.; Lu, C. C.; Peters, J. C. *Proc. Natl. Acad. Sci. U.S.A.* **2006**, *103*, 17107. (c) Rohde, J.-U.; Betley, T. A.; Jackson, T. A.; Saouma, C. T.; Peters, J. C.; Que, L., Jr. *Inorg. Chem.* **2007**, *46*, 5720.

(25) (a) Meyer, K.; Bill, E.; Mienert, B.; Weyhermuller, T.; Wieghardt, K. *J. Am. Chem. Soc.* **1999**, *121*, 4859. (b) Grapperhaus, C. A.; Mienert, B.; Bill, E.; Weyhermüller, T.; Wieghardt, K. *Inorg. Chem.* **2000**, *39*, 5306. (c) Aliaga-Alcalde, N.; DeBeer George, S.; Mienert, B.; Bill, E.; Wieghardt, K.; Neese, F. *Angew. Chem., Int. Ed.* **2005**, *44*, 2908.

(26) Berry, J. F.; Debeer George, S.; Neese, F. *Phys. Chem. Chem. Phys.* **2008**, *10*, 4361.
(27) Berry, J. F.; Bill, E.; Bothe, E.; DeBeer George, S.; Mienert, B.; Neese, F.; Wieghardt, K. *Science* **2006**, *312*, 1937.
(28) Wagner, W. D.; Nakamoto, K. *J. Am. Chem. Soc.* **1989**, *111*, 1590.
(29) Vogel, C.; Heinemann, F. W.; Sutter, J.; Anthin, C.; Meyer, K. *Angew. Chem., Int. Ed.* **2008**, *47*, 2681.
(30) (a) Scepaniak, J. J.; Fulton, M. D.; Bontchev, R. P.; Duesler, E. N.; Kirk, M. L.; Smith, J. M. *J. Am. Chem. Soc.* **2008**, *130*, 10515. (b) Scepaniak, J. J.; Young, J. A.; Bontchev, R. P.; Smith, J. M. *Angew. Chem., Int. Ed.* **2009**, *48*, 3158. (c) Scepaniak, J. J.; Harris, T. D.; Vogel, C. S.; Sutter, J.; Meyer, K.; Smith, J. M. *J. Am. Chem. Soc.* **2011**, *133*, 3824. (d) Scepaniak, J. J.; Vogel, C. S.; Khusniyarov, M. M.; Heinemann, F. W.; Meyer, K.; Smith, J. M. *Science* **2011**, *331*, 1049.
(31) Schlangen, M.; Neugebauer, J.; Reiher, M.; Schroder, D.; Lopez, J. P.; Haryono, M.; Heinnemann, F. W.; Grohmann, A.; Schwarz, H. *J. Am. Chem. Soc.* **2008**, *130*, 4285.
(32) (a) Lucas, R. L.; Powell, D. R.; Borovik, A. S. *J. Am. Chem. Soc.* **2005**, *127*, 11596. (b) Eckert, N. A.; Vaddadi, S.; Stoian, S.; Lachicotte, R. J.; Cundari, T. R.; Holland, P. L. *Angew. Chem.* **2006**, *118*, 7022; *Angew. Chem., Int. Ed.* **2006**, *45*, 6868. (c) Sastri, C. V.; Lee, J.; Oh, K.; Lee, Y. J.; Lee, J.; Jackson, T. A.; Ray, K.; Hirao, H.; Shin, W.; Halfen, J. A.; Kim, J.; Que, L., Jr.; Shaik, S.; Nam, W. *Proc. Natl. Acad. Sci. U.S.A.* **2007**, *104*, 19181.
(33) (a) Hirao, H.; Kumar, D.; Que, L., Jr.; Shaik, S. *J. Am. Chem. Soc.* **2006**, *128*, 8590. (b) Hirao, H.; Que, L., Jr.; Nam, W.; Shaik, S. *Chem.—Eur. J.* **2008**, *14*, 1740. (c) Bukowski, M. R.; Koehntop, K. D.; Stubna, A.; Bominaar, E. L.; Halfen, J. A.; Münck, E.; Nam, W.; Que, L., Jr. *Science* **2005**, *310*, 1000.
(34) Tang, H.; Li, Z.; Yang, Y. H.; Zhao, Y.; Wan, S. Q.; Liu, H. L.; Huang, X. R. *J. Comput. Chem.* **2012**, *33*, 1448.
(35) Neese, F. *ORCA—An ab Initio, Density Functional and Semiempirical Program Package, Version 2.8ed.*; University Bonn: Bonn, Germany, 2010.
(36) Weigend, F.; Ahlrichs, R. *Phys. Chem. Chem. Phys.* **2005**, *7*, 3297.
(37) (a) Becke, A. D. *J. Chem. Phys.* **1993**, *98*, 5648. (b) Lee, C. T.; Yang, W. T.; Parr, R. G. *Phys. Rev. B* **1988**, *37*, 785.
(38) Schäfer, A.; Huber, C.; Ahlrichs, R. *J. Chem. Phys.* **1994**, *100*, 5829.
(39) Neese, F.; Wennmohs, F.; Hansen, A.; Becker, U. *Chem. Phys.* **2009**, *356*, 98.
(40) (a) Eichkorn, K.; Treutler, O.; Ohm, H.; Häser, M.; Ahlrichs, R. *Chem. Phys. Lett.* **1995**, *240*, 283. (b) Eichkorn, K.; Weigend, F.; Treutler, O.; Ahlrichs, R. *Theor. Chem. Acc.* **1997**, *97*, 119. (c) Eichkorn, K.; Treutler, O.; Ohm, H.; Häser, M.; Ahlrichs, R. *Chem. Phys. Lett.* **1995**, *242*, 652.
(41) (a) Neese, F. *J. Inorg. Biochem.* **2006**, *100*, 716. (b) Berry, J. F.; Bill, E.; Bothe, E.; Neese, F.; Wieghardt, K. *J. Am. Chem. Soc.* **2006**, *128*, 13515.
(42) Weigend, F.; Häser, M.; Patzelt, H.; Ahlrichs, R. *Chem. Phys. Lett.* **1998**, *294*, 143.
(43) Weigend, F.; Kohn, A.; Hattig, C. *J. Chem. Phys.* **2002**, *116*, 3175.
(44) (a) Grimme, S.; Antony, J.; Ehrlich, S.; Krieg, H. J. *Chem. Phys.* **2010**, 132. (b) Grimme, S. *J. Comput. Chem.* **2004**, *25*, 1463. (c) Grimme, S. *J. Comput. Chem.* **2006**, *27*, 1787.
(45) Adamo, C.; Barone, V. *J. Chem. Phys.* **1999**, *110*, 6158.
(46) Schöneboom, J. C.; Neese, F.; Thiel, W. *J. Am. Chem. Soc.* **2005**, *127*, 5840.
(47) (a) Ogliaro, F.; Harris, N.; Cohen, S.; Filatov, M.; de Visser, S. P.; Shaik, S. *J. Am. Chem. Soc.* **2000**, *122*, 8977. (b) de Visser, S. P.; Ogliaro, F.; Sharma, P. K.; Shaik, S. *J. Am. Chem. Soc.* **2002**, *124*, 11809. (c) de Visser, S. P. *J. Am. Chem. Soc.* **2010**, *132*, 1087. (d) de Visser, S. P.; Kumar, D.; Cohen, S.; Shacham, R.; Shaik, S. *J. Am. Chem. Soc.* **2004**, *126*, 8362. (e) Groves, J. T.; McClusky, G. A. *J. Am. Chem. Soc.* **1976**, *98*, 859.
(48) (a) Su, J.; Groves, J. T. *J. Am. Chem. Soc.* **2009**, *131*, 12979. (b) Filatov, M.; Harris, N.; Shaik, S. *Angew. Chem., Int. Ed.* **1999**, *38*, 3510. (c) Schoneboom, J. C.; Lin, H.; Reuter, N.; Thiel, W.; Cohen, S.; Ogliaro, F.; Shaik, S. *J. Am. Chem. Soc.* **2002**, *124*, 8142. (d) Ogliaro, F.; de Visser, S. P.; Cohen, S.; Sharma, P. K.; Shaik, S. *J. Am. Chem. Soc.* **2002**, *124*, 2806.
(49) Lonsdale, R.; Harvey, J. N.; Mulholland, A. J. *J. Phys. Chem. Lett.* **2010**, *1*, 3232.
(50) Chen, H.; Lai, W. Z.; Shaik, S. *J. Phys. Chem. Lett.* **2010**, *1*, 1533.
(51) Siegbahn, P. E. M.; Blomberg, M. R. A.; Chen, S.-L. *J. Chem. Theory Comput.* **2010**, *6*, 2040.
(52) (a) Janardanan, D.; Wang, Y.; Schyman, P.; Que, L., Jr.; Shaik, S. *Angew. Chem., Int. Ed.* **2010**, *49*, 3342. (b) Shaik, S.; Chen, H.; Janardanan, D. *Nat. Chem.* **2011**, *3*, 19.
(53) (a) Mayer, J. M. *Acc. Chem. Res.* **1998**, *31*, 441. (b) Mayer, J. M. *Annu. Rev. Phys. Chem.* **2004**, *55*, 363. (c) Mader, E. A.; Manner, V. W.; Markle, T. F.; Wu, A.; Franz, J. A.; Mayer, J. M. *J. Am. Chem. Soc.* **2009**, *131*, 4335.
(54) Borovik, A. S. *Chem. Soc. Rev.* **2011**, *40*, 1870.
(55) de Visser, S. P.; Latifi, R.; Tahsini, L.; Nam, W. *Chem.—Asian J.* **2011**, *6*, 493.
(56) de Visser, S. P.; Tahsini, L.; Nam, W. *Chem.—Eur. J.* **2009**, *15*, 5577.
(57) Prokop, K. A.; de Visser, S. P.; Goldberg, D. P. *Angew. Chem., Int. Ed.* **2010**, *49*, 5091.
(58) Kumar, D.; Karamzadeh, B.; Sastry, G. N.; de Visser, S. P. *J. Am. Chem. Soc.* **2010**, *132*, 7656.